Electronic Supplementary Information

Iron(III) ion-assisted transformation of ZIF-67 to self-supported Fe$_x$Co-layered double hydroxide for improved water oxidation

Priyanka Maurya,[a] Ved Vyas,[a]Abhay Narayan Singh,[b] Arindam Indra[a]*

[a]Department of Chemistry, Indian Institute of Technology (BHU), Varanasi-221005, U.P, India. E- mail: arindam.chy@iitbhu.ac.in

[b]School of Material Science and Technology, Indian Institute of Technology (BHU), Varanasi- 221005, U.P, India

Chemicals

Cobalt chloride hexahydrate and cobalt nitrate hexahydrate were purchased from Sigma Aldrich (99.9%). Urea (99.5%), ammonium fluoride (98%), ferric nitrate nonahydrate, zinc nitrate hexahydrate, and 2-methyl imidazole were bought from SRL, India. All chemicals were used without any further purification. Nickel foam was purchased from AXYS technology, India. Double distilled water was used for all the experiments and electrochemical measurements.

Instrument

The crystallinity and phase identification of the synthesized catalysts were confirmed by room temperature X-ray diffraction (Rigaku Miniflex 600) using Cu-K alpha radiation (λ=1.5418 A^o). The IR spectra were recorded at Nicolet iS5 FTIR spectrometer in attenuated total reflection (ATR) mode in the range between 400-4000 cm^{-1}. The XPS spectra have been measured using a Thermo Fisher Scientific instrument with Al K-alpha radiation operated at 150 W. Microstructure and compositional analyses of the prepared materials were examined with the help of Field emission scanning electron microscopy (Nova Nano SEM 450) equipped with an EDS System and the interlayer d-spacing of the synthesized catalysts was obtained by taking HR-TEM images (FEI TECNAI G2 20 TWIN) operated at 300 kV.

Synthesis of catalysts
Activation of nickel foam[S1]

A piece of nickel foam (1 cm x 2 cm) was first washed with 3.0 M HCl under ultrasonication, followed by washing with water and ethanol repeatedly. The activated nickel foam was dried in an air oven for 12 h at 50 ^{o}C for further use.

Synthesis of cobalt hydroxide carbonate template on nickel foam (Co-HC@NF)[S2]

The precursor compound CoCl$_2$.6H$_2$O (2 mmol), NH$_4$F (4 mmol), and urea (10 mmol) were dissolved in 12 mL water. The reaction mixture was stirred at room temperature for 30

minutes and transferred into a 50 mL Teflon line autoclave. A piece of activated nickel foam was immersed vertically into the solution to dip 1 cm^2 geometrical surface area. The autoclave was sealed and heated in an electric oven at 120 °C for 5 h. After natural cooling to room temperature, cobalt hydroxide carbonate (Co-HC) coated nickel foam was taken out and washed with water and ethanol twice followed by drying at 60 °C for 12 h.

Synthesis of ZIF-67@NF[S3]

5 mmol of 2-methyl imidazole (2-MeIm) was dissolved in 5 mL methanol in a 15 mL glass vial. Co-HC@NF was immersed vertically in the as-prepared solution of 2-MeIm. The glass vial was capped and kept at room temperature for 12 h. After 12 h, a purple-colored ZIF-67 deposited NF was obtained that indicates the conversion of Co-HC@NF to ZIF-67@NF. The as-obtained ZIF-67@NF was washed several times with methanol to remove unreacted 2-MeIm and dried at 60 °C for 12 h.

Synthesis of Fe$_{0.4}$ Co-LDH@NF[S4]

0.04 mmol of Fe(NO$_3$)$_3$.9H$_2$O was dissolved in a mixed solution of isopropanol and ethylene glycol (8:2). The solution was transferred into a Teflon-lined autoclave. The as-synthesized ZIF-67@NF was vertically immersed into the reaction mixture, and the autoclave was sealed. The sealed autoclave was heated at 120 °C for 5 h in an air oven. The reaction was allowed to cool down to room temperature. Fe$_{0.4}$Co-LDH@NF was dried at 60 °C for overnight.

The large electrochemical active surface area, flexible layered structure, controllable compositions, and availability of the active sites of LDHs result in improved electrochemical activity.

Synthesis of Co-LDH@NF[S4]

Co-LDH@NF was synthesised following the synthesis process of Fe$_{0.4}$Co-LDH@NF by replacing Fe(NO$_3$)$_3$.9H$_2$O with 0.04 mmol of Co(NO$_3$)$_2$.6H$_2$O.

Synthesis of ZnCo-LDH@NF[S4]

ZnCo-LDH@NF was synthesised following the synthesis process of Fe$_{0.4}$Co-LDH@NF only by replacing Fe(NO$_3$)$_3$.9H$_2$O with 0.04 mmol of Zn(NO$_3$)$_2$.6H$_2$O.

Synthesis of iron cobalt hydroxide carbonate on nickel foam (Fe$_{0.4}$Co-HC@NF)

The precursor compounds Fe(NO$_3$)$_3$.9H$_2$O (0.4 mmol), CoCl$_2$.6H$_2$O (1.6 mmol), NH$_4$F (4 mmol), and urea (10 mmol) were dissolved in 12 mL water, stirred at room temperature for 30 minutes, and the mixture was transferred into a 50 mL Teflon line autoclave. Activated nickel foam was dipped into the solution to cover 1 cm^2 geometrical area. The autoclave was sealed and placed in a preheated electric oven (120 °C) to continue the reaction for 5 h. After natural cooling to room temperature, Fe$_{0.4}$Co-HC@NF was taken out, washed with water and ethanol and dried at 60 °C for 12 h.

Synthesis of Fe$_{0.4}$Co-ZIF-67@NF[S3]

5 mmol 2-MeIm was dissolved in 5 mL methanol and Fe$_{0.4}$Co-HC@NF was immersed vertically, and reacted for 12 h at room temperature. The as-obtained Fe$_{0.4}$Co-ZIF-67@NF

was washed with methanol and dried at 60 °C for 12 h.

Table S1: Details of the catalysts

Catalyst	Precursor	Amount of salt
Co-LDH@NF	ZIF-67@NF	$CoCl_2.6H_2O$ (0.4 mmol)
ZnCo-LDH@NF	ZIF-67@NF	$Zn(NO_3)_2.6H_2O$ (0.4 mmol)
$Fe_{0.1}Co$-LDH@NF	ZIF-67@NF	$Fe(NO_3)_3.9H_2O$ (0.1 mmol)
$Fe_{0.2}Co$-LDH@NF	ZIF-67@NF	$Fe(NO_3)_3.9H_2O$ (0.2 mmol)
$Fe_{0.3}Co$-LDH@NF	ZIF-67@NF	$Fe(NO_3)_3.9H_2O$ (0.3 mmol)
$Fe_{0.4}Co$-LDH@NF	ZIF-67@NF	$Fe(NO_3)_3.9H_2O$ (0.4 mmol)
$Fe_{0.5}Co$-LDH@NF	ZIF-67@NF	$Fe(NO_3)_3.9H_2O$ (0.5mmol)

Electrochemical measurements:

The oxygen evolution experiments were performed in a single-compartment three-electrode electrochemical cell in 1.0 M aqueous KOH solution (pH 13.57). Catalyst-deposited nickel foam was used as the working electrode, and Pt wire was used as the counter electrode. Ag/AgCl electrode was used as the reference electrode.

The applied potential was represented against reversible hydrogen electrode (RHE) by using the formula: $E(RHE) = E(Ag/AgCl) + 0.197 + 0.059pH$.

Chronoamperometric measurements were carried out in 1.0 M KOH at a constant potential. Correction for iR losses was performed for all the CV and LSV measurements whereas chronoamperometric data were represented without any iR correction.
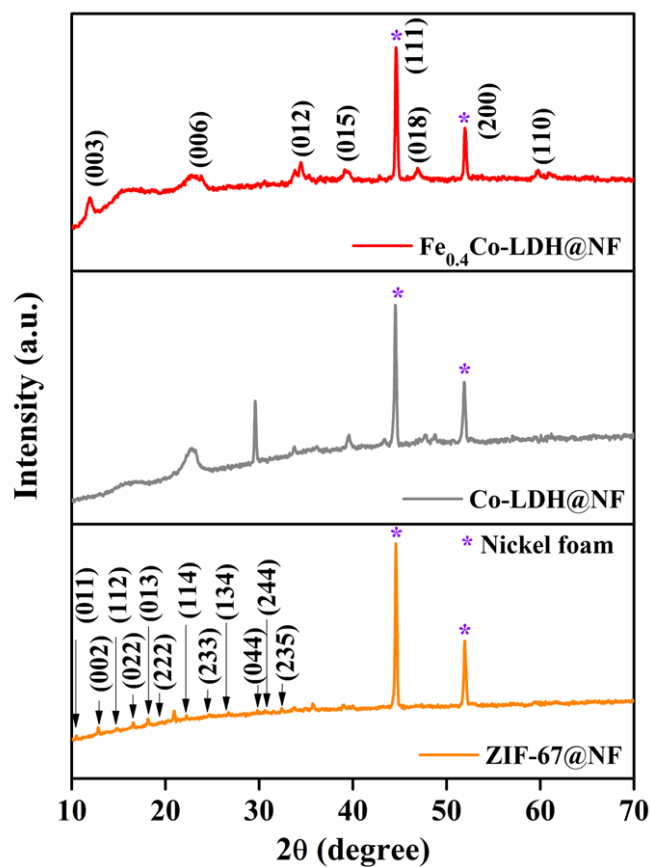
Figure S1. (Top) The powder X-ray diffraction pattern of $Fe_{0.4}Co$-LDH@NF is in good agreement with the rhombohedral crystal of cobalt hydroxide (JCPDS card No. 50-0235).The * marked peaks are assigned for nickel foam.(Middle)The powder X-ray diffraction pattern of Co-LDH@NF and (Down) The powder X-ray diffraction pattern of ZIF-67@NF.
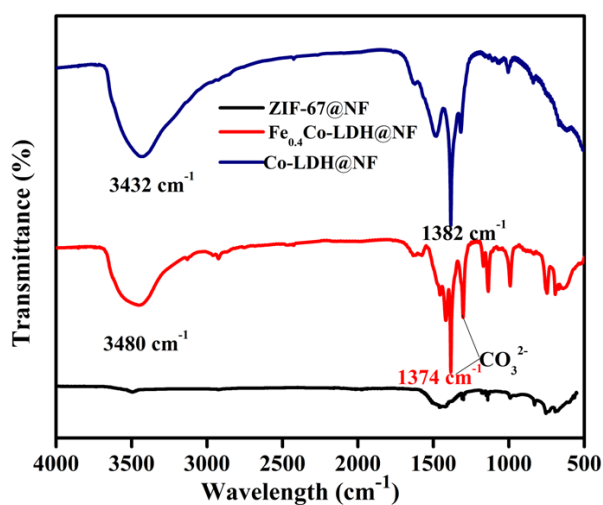

Figure S2. Fourier transformed infrared (FTIR) spectra of ZIF-67@NF, Co-LDH@NF and $Fe_{0.4}$Co-LDH@NF.
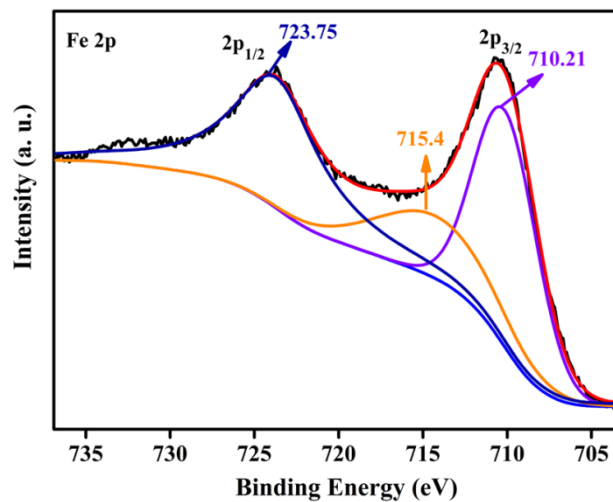
Figure S3. Fe 2p X-ray photoelectron spectrum of $Fe_{0.4}Co$-LDH. The Fe 2p spectrum was deconvoluted into two peaks with binding energy 724.15 eV and 710.61 eV corresponding to $2p_{1/2}$ and $2p_{3/2}$.[S5]
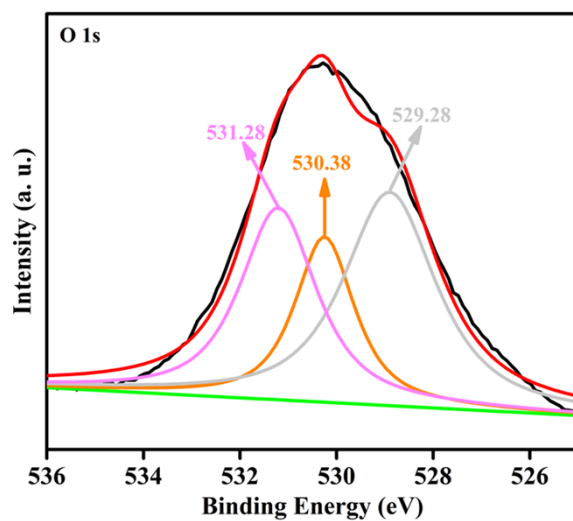

Figure S4. The O 1s XPS was fitted into three peaks corresponding to the oxygen of water (531.28 eV), surface oxygen (~530.38 eV) and Co/Fe-O bond (529.28 eV)[S5]
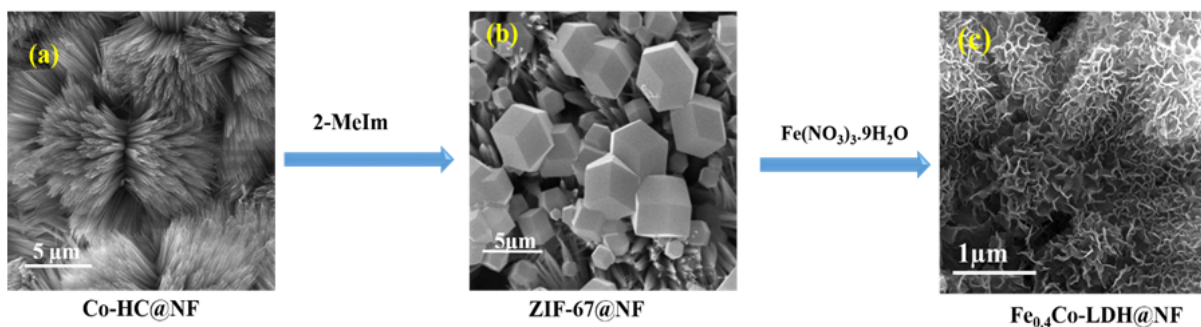
Figure S5. SEM images of (a) Co-HC@NF (b) ZIF-67@NF, and (c) $Fe_{0.4}Co$-LDH@NF. The use of Co-HC as the template led to the controlled growth of ZIF-67 on the surface of Co-HC. This results in a distinct interaction between the nickel foam and ZIF-67, which may affect its conversion into $Fe_{0.4}Co$-LDH by tuning the thickness, electrochemical surface area, and number of active sites.
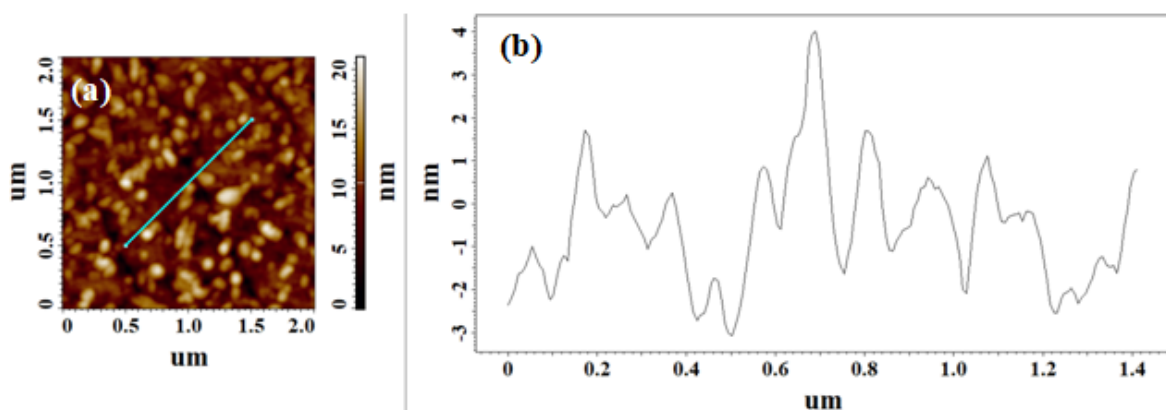

Figure S6. (a) AFM image of $Fe_{0.4}Co$-LDH@NF and (b) corresponding height profile showing the ~ 4 nm thickness of the nanosheets. The thin nanosheets offer a large number of active sites with coordinative and electronic unsaturation for substrate binding as well as high active surface area.
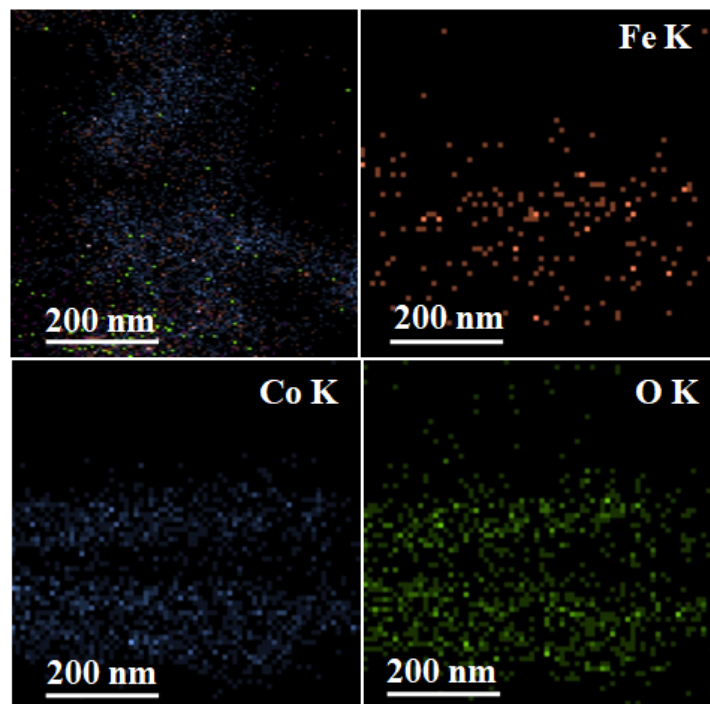
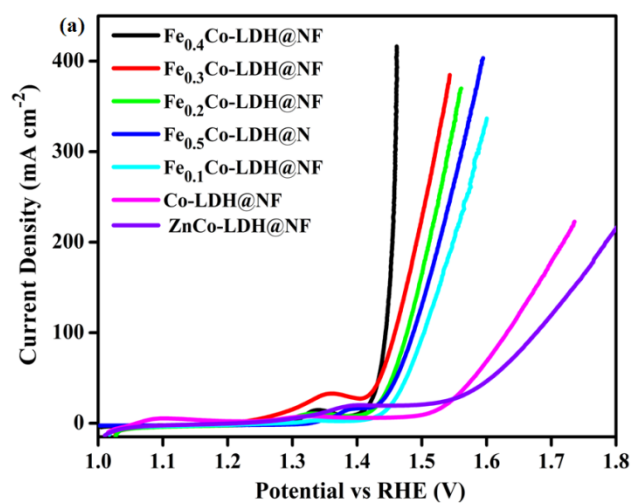**Figure S7.** Elemental mapping of $Fe_{0.4}Co$-LDH@NF showing the distribution of the elements Fe, Co and O.

Figure S8. LSV profiles for OER of Fe_xCo-LDH@NF catalysts having different amount of Fe(III) in the structure.
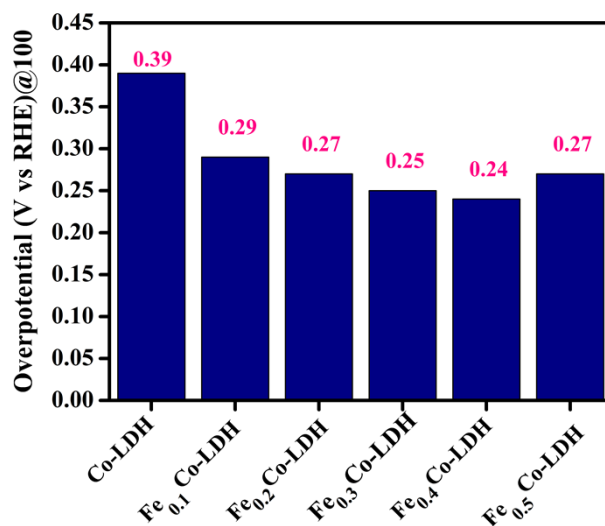
Figure S9. Comparison of the overpotential of the catalysts to reach a current density of 100 mA cm^{-2}.

A high valence state of transition metal ions (Co^{III}) generates a larger number of active oxygenated species and adsorbs more OH$^-$ ions on its catalytic surface to enhance the OER activity. In a high spin octahedral field, Fe^{III} and Co^{II} have the electronic configuration $t_{2g}^3e_g^2$ and $t_{2g}^5e_g^2$, respectively. On the other hand, having a low spin state, the t_{2g} orbitals of Co^{III} are fully occupied, resulting a weak interaction with bridging O^{2-} due to electron-electron repulsion. Since Co^{II} has one unpaired electron in t_{2g} orbitals, the exchange of partial electron density between Co^{II} and Co^{III} takes place through weak π-donation involving bridging O^{2-}.

Table S2. The OER activities of reported LDHs compared with Fe$_{0.4}$Co-LDH@NF.

Sr. No.	Catalyst	Current density (mA cm^{-2})	Overpotential (mV)	Reference
1	**Fe$_{0.4}$Co-LDH@NF**	**20**	**190**	**This work**
2	CoFe-LDH-Ar@NF	10	299	S6
3	NiCoFe-LDH@CFP	10	239	S7
4	NiCo-LDH nanoplates@CP	10	367	S8
5	CoMoV-LDHs@NF	10	270	S9
6	CoFe-LDH@Cu NWs	10	240	S10
7	H$_2$O-plasma CoFe-LDH	10	232	S11
8	NiCoFe-LDHs/CFC	10	239	S12
9	Ni$_{76}$Co$_{24}$-LDHs@NF	10	293	S13
10	CoNiP/NiFe-LDH	10	210	S14
11	Ni$_3$Co$_3$Fe$_3$LDH	10	290	S15
12	E-CoFe-LDHs	10	300	S16
13	ZnFeCo-LDH	10	221	S17
14	CoMn-LDH nanosheets	10	324	S18
15	NiCo-LDH nanosheets	10	299	S19

Table S3. The OER activities of ZIF derived electrocatalysts compared with $Fe_{0.4}Co$-LDH@NF.

| Sr. No.	Catalyst	Current density (mA cm^{-2})	Overpotential (mV)	Reference
1	**$Fe_{0.4}Co$-LDH@NF**	**20**	**190**	**This work**
2	**ZIF-67@NF**	**20**	**270**	**This work**
3	CoO_x-ZIF	10	318	S20
4	NiCoP/C nanoboxes	10	330	S21
5	Co_3O_4@CoP	10	238	S22
6	Co-P/NC	10	319	S23
7	Co-P/NC/CC	10	330	S24
8	Co_3S_4@MoS_2	10	330	S25
9	M-Co_3O_4/NPC	10	290	S26
10	Fe-Co_3O_4 HHNPs	10	262	S27
11	N-Co_3O_4@NC	10	266	S28
12	Co_3O_4/$NiCo_2O_4$ DSNCs/NF	10	340	S29
13	Co_3O_4/Co-Fe-oxide DSNBs/GCE	10	297	S30
14	Co-NC@CoP-NC/GCE	10	330	S31
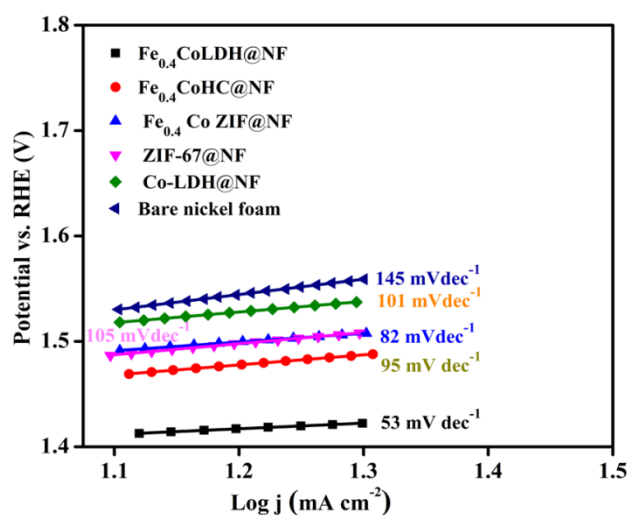
Figure S10. Tafel plots for the oxygen evolution reaction of $Fe_{0.4}Co$-LDH@NF compared with other catalysts. The lowest Tafel slope for $Fe_{0.4}Co$-LDH@NF suggests the fastest OER kinetics for $Fe_{0.4}Co$-LDH@NF.
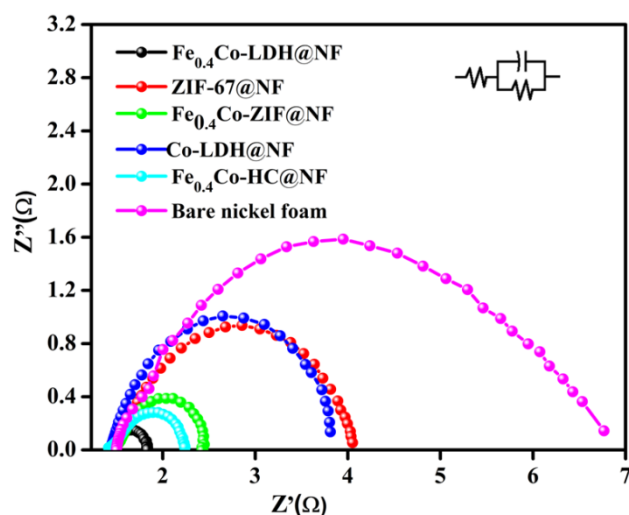
Figure S11. Nyquist plots for the Fe$_{0.4}$Co-LDH@NF, Co-Co-LDH@NF, ZIF-67@NF, Fe$_{0.4}$Co-ZIF@NF, Fe$_{0.4}$Co-HC@NF, and bare nickel foam obtained from electrochemical impedance spectroscopic (EIS) measurements showing lowest charge transfer resistance for Fe$_{0.4}$Co-LDH@NF. The spectra were collected with an anodic polarization potential of 1.48 V vs RHE.

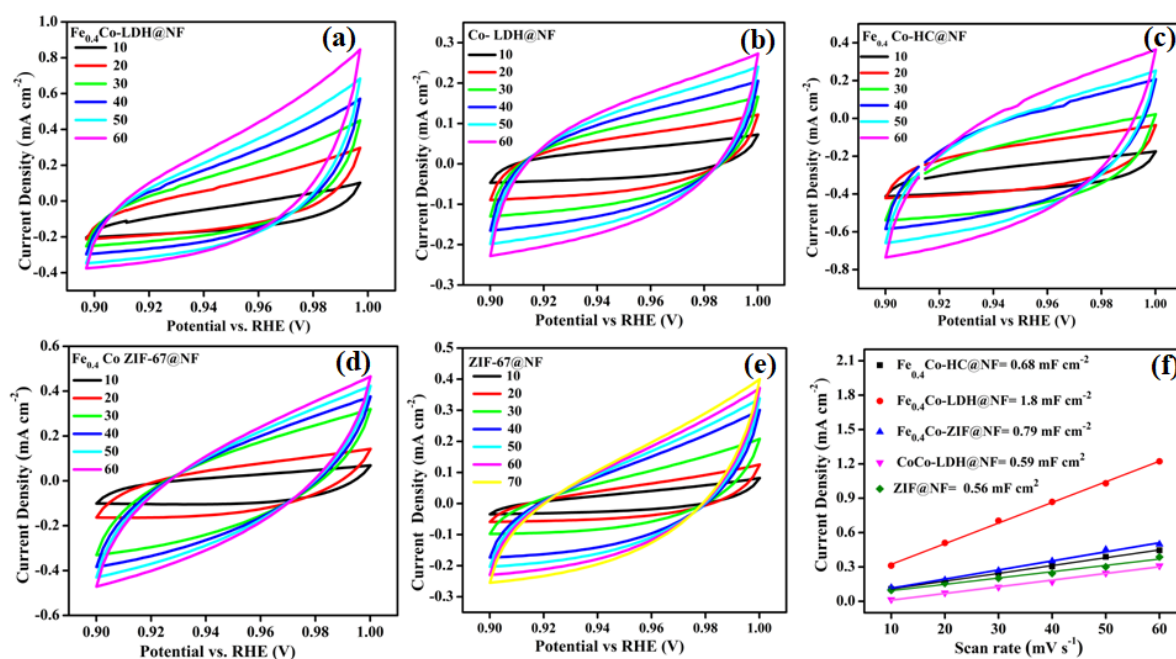**Figure S12.** Determination of double-layer capacitance (C_{dl}) of Fe$_{0.4}$Co-LDH@NF, Co-LDH@NF, Fe$_{0.4}$Co-HC@NF, Fe$_{0.4}$Co-ZIF@NFand ZIF-67@NF by plotting (difference in current density)/2 against scan rate.
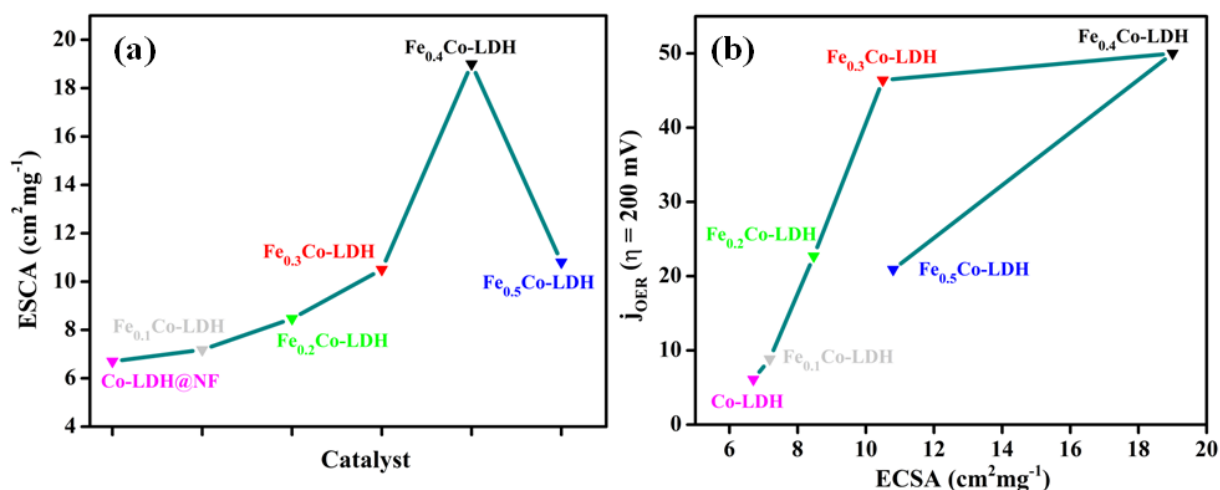
Figure S13. (a) Plot of ECSA *vs* Catalyst Fe_xCo-LDHs@NF. The plot shows that the ECSA is increased up to $Fe_{0.4}Co$-LDH with increase in the iron substitution after that no increment in ECSA is observed. (b) The OER current density of different catalysts attained at 200 mV overpotential plotted against ECSA.

The ECSA of a catalyst is calculated from the double layer capacitance according to the formula:

$$ECSA = C_{dl}/Cs$$

Where C_{dl} is double layer capacitance of the catalyst and Cs is specific capacitance of the material per unit area under identical electrolyte conditions. Cs = 0.040 mF cm^{-2} in 1.0 M KOH based on reported values.[S32]

Table S4: The determination of C_{dl} and ECSA of Fe_xCo-LDH.

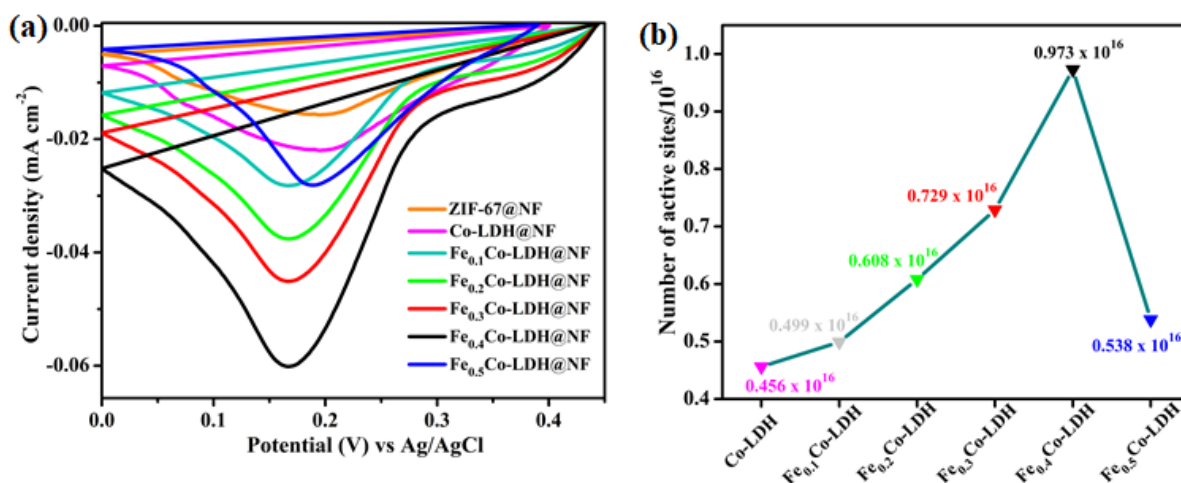| S. No.	Catalyst	C_{dl} (mF cm^{-2})	ECSA (cm^2 mg^{-1})
1	Co-LDH	0.59	6.70
2	$Fe_{0.1}Co$-LDH	0.69	7.18
3	$Fe_{0.2}Co$-LDH	0.78	8.47
4	$Fe_{0.3}Co$-LDH	1.01	10.50
5	$Fe_{0.4}Co$-LDH	1.8	19.00
6	$Fe_{0.5}Co$-LDH	1.02	10.80

Figure S14. (a) Potential vs current density plots showing the reduction peak used for the area integration curve. (b) The number of active sites of $Fe_xCo-LDH@NF$ having different amount of Fe(III).

Equation S1: Determination of surface active sites using area integration of reduction peak[S33, S34]

For $Fe_{0.4}Co-LDH$

Calculated area associated with the reduction peak = 7.79×10^{-6} V A

Hence the associated charge is = 7.799×10^{-6} V A / 0.005 V s^{-1}

$$= 1.559 \times 10^{-3} \text{ A s}$$
$$= 1.559 \times 10^{-3} \text{ C}$$

Now, the number of electron transferred is = 1.559×10^{-3} C / 1.602×10^{-19} C

$$= 0.973 \times 10^{16}$$

Since the reduction of Co^{3+} to Co^{2+} is a single electron transfer reaction, the number of electrons calculated above is the same as the number of surface active sites.

Hence,

The surface-active site that participated in OER is = **0.973×10^{16}**

Equation S2: Calculation of Turn over frequency (TOF) of different catalyst[S33, S34]

$TOF = (j \times N_A) / (4 \times F \times n)$

Where,

j = current density at η = 200 mV

N_A = Avogadro number

F = Faraday constant

n = number of active Co-sites

For $Fe_{0.4}Co-LDH$

$TOF = [(50 \times 10^{-3}) \times (6.023 \times 10^{23})] / [(4) \times (96485) \times (0.973 \times 10^{16})]$

$$= 8.61 \text{ s}^{-1}$$

Table S5: Area under the curve, no. of active site and turnover frequency of Fe_xCo-LDH catalyst.

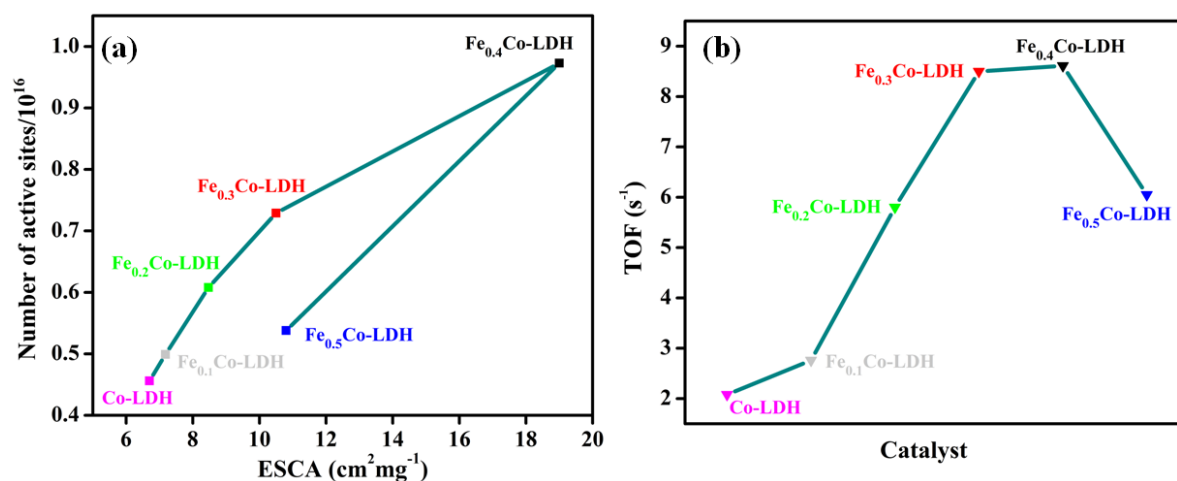| S. No.	Catalyst	Area under the curve (VA)	No. of active site (n)	TOF (s^{-1})
1	Co-LDH	3.656×10^{-6}	0.456×10^{16}	2.08
2	$Fe_{0.1}Co$-LDH	3.997×10^{-6}	0.499×10^{16}	2.76
3	$Fe_{0.2}Co$-LDH	4.874×10^{-6}	0.608×10^{16}	5.80
4	$Fe_{0.3}Co$-LDH	5.849×10^{-6}	0.729×10^{16}	8.50
5	$Fe_{0.4}Co$-LDH	7.799×10^{-6}	0.973×10^{16}	8.61
6	$Fe_{0.5}Co$-LDH	4.310×10^{-6}	0.538×10^{16}	6.00

Figure S15: (a) Plot of the number of active sites *vs* ECSA for Fe_xCo-LDHs@NF. (b) Plot for the turn over frequency (TOF) of catalysts Fe_xCo-LDHs@NF.

The superior OER activity of $Fe_{0.4}Co$-LDH@NF can be explained by (i) modulated electronic structure of the catalyst attained by the introduction of Fe(III) ion in Co-LDH, (ii) increased electrochemical surface area, (iii) improved charge transfer, and (iv) atomic level thickness of the nanosheets.

References

S1.   H. Hu, B. Guan, B. Xiaand X. W. Lou, *J. Am. Chem. Soc.*, 2015, **137**, 5590-5595.

S2.   A. Indra, U. Paik and T. Song, *Angew. Chem. Int. Ed.*, 2018, **57**, 1241-1245.

S3.   Z. Chen, Y. Ha, H. Jia, X. Yan, M. Chen, M. Liu and R. Wu, *Adv. Energy Mater.,* 2019, **9**, 1803918.

S4.　　Y. Lin, H. Wang, C.K. Peng, L. Bu, C. L. Chiang, K. Tian, Y. Zhao, J. Zhao, Y. G. Lin, J. M. Leeand L. Gao, *Small,* 2020, **16**, 2002426.

S5.　　J. Zhao, X. R. Wang, F. W. Chen, C. He, X. J. Wang, Y. P. Li, R. H. Liu, X.-M. Chen, Y. J. Hao, M. Yang and F. T. Li, *Inorg. Chem. Front.*, 2020, **7**, 737.

S6.　　Y. Wang, Y. Zhang, Z. Liu, C. Xie, S. Feng, D. Liu, M. Shao and S. Wang, *Angew. Chem. Int. Ed.*, 2017, **56**, 5867-5871.

S7.　　A.L. Wang, H. Xu, and G.-R. Li, *ACS Energy Lett.*, 2016, **2**, 445-453.

S8.　　H. Liang, F. Meng, M. C. Acevedo, L. Li, A. Forticaux, L. Xiu, Z. Wang, and S. Jin, *Nano Letters*, 2015, **15**, 1421-1427.

S9.　　J. Bao, Z. Wang, J. Xie, and L. Xu, *Chem. Commun.*, 2019, **55**, 3521-3524.

S10.　L. Yu, H. Zhou, J. Sun, F. Qin, D. Luo, L. Xie, F. Yu, J. Bao, Y. Li, Y. Yu, S. Chen and Z. Ren, *Nano Energy*, 2017, **41**, 327-336.

S11.　R. Liu, Y. Wang, D. Liu, Y. Zou and S. Wang, *Adv. Mater.,* 2017, **29**, 1701546.

S12.　A. L. Wang, H. Xu and G. R. Li, *ACS Energy Lett.*, 2016, **1**, 445-453.

S13.　J. Li, W. Xu, R. Li, J. Luo, D. Zhou, S. Li, P. Cheng and D. Yuan, *J. Mater. Sci.,* 2016, **51**, 9287-9295.

S14.　L. Zhou, S. Jiang, Y. Liu, M. Shao, M. Wei and X. Duan, *ACS Appl. Energy Mater.*, 2018, **1**, 623-631.

S15.　A. G. Vargas, J. V. Samperio, M. A. O. Tolentino, N. Nava, N. Castillo, M. J. M. Hernandez and E. Reguera, *J. Mater. Sci.*, 2018, **53**, 4515-4526.

S16.　P. Zhou, Y. Wang, C. Xie, C. Chen, H. Liu, R. Chen, J. Huo and S. Wang, *Chem. Commun.*, 2017, **53**, 11778-11781.

S17.　J. Han, J. Zhang, T. Wang, Q. Xiong, W. Wang, L. Cao, and B. Dong, *ACS Sustain. Chem. Eng.*, 2019, **7**, 13105-13114.

S18.　F. Song and X. Hu, *J. Am. Chem. Soc.*, 2014, **136**, 16481-16484.

S19.　Y. Liu, M. Zhang, D. Hu, R. Li, K. Hu and K. Yan, *ACS Appl. Energy Mater.,* 2019, **2,** 1162-1168.

S20.　S. Dou, C.L. Dong, Z. Hu, Y. C. Huang, J. l. Chen, L. Tao, D. Yan, D. Chen, S. Shen, S. Chou, and S. Wang, *Adv. Funct. Mater.,* 2017, **27**, 1702546.

S21.　P. He, X. Y. Yu and X. W. Lou,*Angew. Chem. Int. Ed.*, 2017, **56**, 3897-3900.

S22.　J. Zhou, Y. Dou, A. Zhou, R. M. Guo, M. J. Zhao and J. R. Li, *Adv. Energy Mater.,* 2017, **7**, 1602643.

S23.　B. You, N. Jiang, M. Sheng, S. Gul, J. Yano and Y. Sun, *Chem. Mater.*, 2015, **27**, 7636-7642.

S24.   X. Liu, J. Dong, B. You and Y. Sun, *RSC Adv.*, 2016, **6**, 73336-73342.

S25.   Y. Guo, J. Tang, H. Qian, Z. Wang and Y. Yamauchi, *Chem. Mater.,* 2017, **29**, 286–5573.

S26.   X. Yang, J. Chen, Y. Chen, P. Feng, H. Lai, J. Li and X. Luo, *Nano-Micro Lett.*, 2017, **10**, 15.

S27.   S. L. Zhang, B.Y. Guan, X. F. Lu, S. Xi, Y. Du and X.W. Lou, *Adv. Mater.*, 2020, **32**, 2002235.

S28.   Z. Wang, W. Xu, X. Chen, Y. Peng, Y. Song, C. Lv, H. Liu, J. Sun, D. Yuan, X. Li, X. Guo, D. Yang and L. Zhang, *Adv. Funct. Mater.*, 2019, **29**, 1902875.

S29.   H. Hu, B. Guan, B. Xia and X. W. Lou, *J. Am. Chem. Soc.,* 2015, **137**, 5590–5595.

S30.   X. Wang, L. Yu, B. Y. Guan, S. Song and X. W. Lou, *Adv. Mater.* 2018, 1801211.

S31.   X. Li, Q. Jiang, S. Dou, L. Deng, J. Huo and S. Wang, *J. Mater. Chem. A,* 2016, **4**, 15836–15840.

S32.   C. C. L. McCrory, S. Jung, J. C. Peters and T. F. Jaramillo, *J. Am. Chem. Soc.* 2013, **135**, 16977−16987.

S33.   S. Anantharaj and S. Kundu, *ACS Energy Lett*. 2019, **4**, 1260-1264.

S34.   S. Anantharaj, S. R. Ede, K. Karthick, S. S. Sankar, K. Sangeetha, P. E. Karthik, S. Kundu, *Energy Environ. Sci.* 2018, **11**, 744-771.